



Two scenarios of advective washing-out of localized convective patterns under frozen parametric disorder

Denis S. Goldobin

Institute of Continuous Media Mechanics UB RAS, 1 Akad. Koroleva street, 614013 Perm, Russia

Theoretical Physics Department, Perm State University, 15 Bukireva street, 614990 Perm, Russia

Abstract

The effect of spatial localization of states in distributed parameter systems under frozen parametric disorder is well known as the Anderson localization and thoroughly studied for the Schrödinger equation and linear dissipation-free wave equations. Some similar (*or* mimicking) phenomena can occur in dissipative systems such as the thermal convection ones. Specifically, many of these dissipative systems are governed by a modified Kuramoto–Sivashinsky equation, where the frozen spatial disorder of parameters has been reported to lead to excitation of localized patterns. Imposed advection in the modified Kuramoto–Sivashinsky equation can affect the localized patterns in a nontrivial way; it changes the localization properties and suppresses the pattern. The latter effect is considered in this paper by means of both numerical simulation and model reduction, which turns out to be very seminal. Two possible bifurcation scenarios of advective suppression (“washing-out”) of localized patterns are revealed and characterised.

Keywords: modified Kuramoto–Sivashinsky equation, frozen parametric disorder, localized patterns, advection, bifurcation scenario

1. Introduction

The phenomenon of localization of linear waves in media with frozen disorder of distributed parameters—Anderson localization [1, 2]—is one of the most distinguishable findings in mathematical physics in the 20th century. The phenomenon has drawn attention and earned its name after the discovery of the effect in quantum mechanics [1]. Later on, the Anderson localization has been widely studied in quantum optics (*e.g.*, see [3, 4]) and diverse branches of classical physics; for instance, in wave optics [5] and acoustics [6]. The phenomenon has been well understood mathematically for the Schrödinger equation and linear dissipation-free wave equations [2, 7, 8, 9].

The absence of dissipation in the system is essential for the very concept of the Anderson localization. However, for an active/dissipative medium with frozen parametric disorder the mathematical formulation of some problems can be formally very similar to that of the Anderson localization [10]. Nonetheless, to the authors’ knowledge, the localization-related aspects in the behaviour of dissipative systems with frozen parametric disorder have been studied only in [10, 11, 12], while few other authors considered the effect of disorder on the linear instability threshold of the base state of the system [13, 14].

Email address: Denis.Goldobin@gmail.com (Denis S. Goldobin)

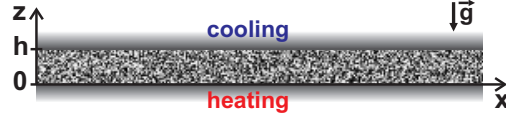


Figure 1: Fluid-saturated porous layer heated from below and the coordinate frame

Localized patterns in dissipative systems

A fluid-saturated horizontal porous layer with nearly thermally insulating boundaries heated from below (see Fig. 1) is an example of the system where frozen disorder of distributed parameters is physically plausible; it can be related to the imperfectness of the homogeneity of the solid matrix packing and applied heat flux. For the case of a thin layer, the temperature perturbation is nearly uniform along the vertical coordinate, $\theta = \theta(x, y, t)$, and its dynamics is governed by equation (see [15])

$$\dot{\theta} + \vec{u} \cdot \nabla \theta + \Delta^2 \theta - \nabla \cdot (\nabla \theta (\nabla \theta)^2 - q(x, y) \nabla \theta) = 0,$$

where $q(x, y)$ is the relative deviation of the local Rayleigh–Darcy number from the critical value of the homogeneous layer and $\vec{u}(x, y)$ is an imposed advective through-flow uniquely determined by the lateral boundary conditions and the conservation law $\nabla \cdot \vec{u} = 0$. Positive $q(x, y)$ means the local excess over the instability threshold of the uniform system; q can be referred to as “supercriticality”.

We will consider the case of a system uniform along the y -coordinate. Then the governing equation turns into a modified Kuramoto–Sivashinsky equation

$$\dot{\theta} = \left(-u\theta - \theta_{xxx} - q(x)\theta_x + (\theta_x)^3 \right)_x, \quad (1)$$

where u is the x -component of the imposed advection (through-flow) velocity and must be constant. Here, we would like to emphasize that Eq. (1) is a typical governing equation for the pattern formation in systems with symmetry $\theta \leftrightarrow -\theta$ (this symmetry emerges also in the systems where θ is an amplitude of a mode oscillating in space or time); for instance, see [16, 17, 18, 19, 20].

The frozen parametric disorder is represented by a δ -correlated Gaussian noise:

$$q(x) = q_0 + \xi(x), \quad \langle \xi(x) \rangle = 0, \quad \langle \xi(x) \xi(x') \rangle = 2\sigma^2 \delta(x - x'), \quad (2)$$

where q_0 is the mean supercriticality, σ is the noise strength. The noise strength σ may be set to 1 by means of the rescaling $(x, t, q) \rightarrow (\sigma^{-2/3}x, \sigma^{-8/3}t, \sigma^{4/3}q)$.

For a porous layer, the fluid velocity field of the convective flow is

$$\vec{v} = \frac{\partial \Psi}{\partial z} \vec{e}_x - \frac{\partial \Psi}{\partial x} \vec{e}_z, \quad \Psi = f(z) \psi(x, t), \quad (3)$$

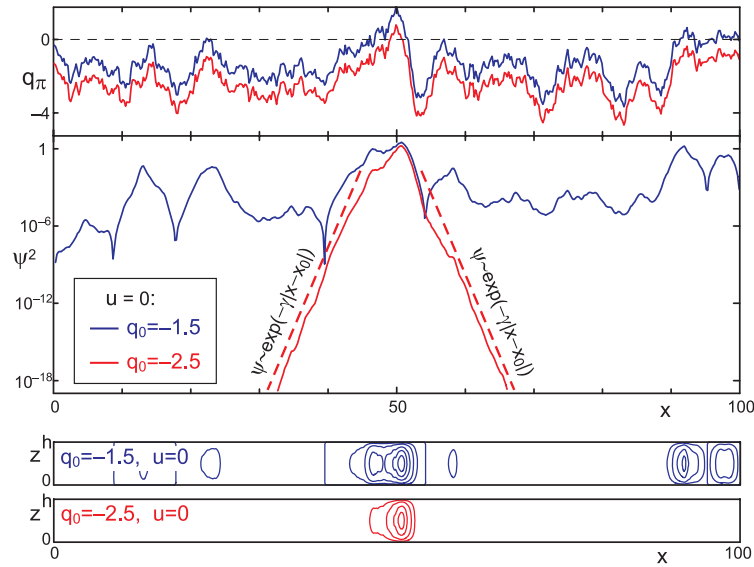
where $\psi(x, t) = \theta_x(x, t)$ is the stream function amplitude and $f(z) = 3\sqrt{35}\sigma^{-1}h^{-3}z(h-z)$, h is the layer thickness [15]. Notice, for different convective systems function $f(z)$ will be different, but the relation $\psi(x, t) = \theta_x(x, t)$ will be preserved.

As demonstrated in [10], for $u = 0$ and $q_0 < 0$ only time-independent patterns are stable. For moderate negative values of q_0 the system state turns into a set of separate localized convective patterns (Fig. 2). The localization of each individual pattern is exponential; at the distance from the pattern centre x_0 the field $\psi \propto \exp(-\gamma|x - x_0|)$, where γ is the localization exponent. In [11, 12] the localization properties of these patterns have been shown to drastically influence the diffusive transport of a passive scalar in the system.

Noise realizations are visually represented in plots with

$$q_l(x) \equiv \frac{1}{l} \int_{x-l/2}^{x+l/2} q(x_1) dx_1.$$

When at the point x the value of $q_l(x)$ is positive for large enough l ($l \sim 1$), one may expect a convective flow probably to arise in the vicinity of this point, while in the domain of negative q_l the convective flow is averagely damped.

Figure 2: Localized pattern and convective flows for $u = 0$

Naturally, as the magnitude of negative q_0 increases for a given realization $\xi(x)$, the localized convective patterns become more rare in space.

In [10], advection u has been revealed to have a significant influence on the localization properties of patterns. However, the effect of advection was considered there only for small values of u , while the strong advection must also suppress the localized convective patterns by washing-out the temperature perturbation from the excitation zone. In this paper we study possible bifurcation scenarios of such a washing-out. Specifically, we firstly argue that the temporal dynamics of the system under consideration is infinitely smooth. Secondly, we provide observations on the possible scenarios with extensive numerical simulations. Thirdly, we derive null-dimensional model reduction equations admitting analytical treatment and find the picture of possible bifurcation scenarios, which is identical to the one reported with numerics.

2. Two scenarios of washing-out

Firstly, let us infer what kind of behaviour can be expected as the advection strength u increases. On the one hand, for $u = 0$ all patterns are time-independent, which should be preserved by continuity at least for small but finite u . On the other hand, for $u > 0$ and homogeneous $q(x) = q_0$, due to the space-shift symmetry, one can eliminate the u -term from Eq. (1) by choosing the coordinate frame moving with velocity u . Hence, for a homogeneous $q(x) = q_0$ and nonzero u , one should observe space-periodic patterns moving with velocity u , which means oscillations at a given point x . The frozen noise breaks the space-shift symmetry and, moreover, for the conditions of excitation of localized convective patterns the patterns are tied to their excitation centres. Thus, for small u the frozen disorder enforces the oscillating patterns to become time-independent. Nonetheless, for some conditions one can expect to observe oscillatory patterns, while the existence of the conditions, for which a convective pattern remains time-independent until it is completely suppressed by advection u , is not *a priori* excluded. Thus, we can generally expect at least two scenarios: (i) a scenario with only time-independent patterns and (ii) scenario with bifurcation involving appearance of stable oscillatory regimes.

2.1. Smoothness of temporal evolution of system (1)

If we expect existence of stable time-dependent patterns, some general explanations about the temporal evolution of system (1) with frozen δ -correlated noise $\xi(x)$ are due. Indeed, δ -correlated noise in Eq. (1) makes $\theta(x, t)$ differentiable with respect to x only twice, as $\theta_{xxx} \sim \sigma \xi(x) \theta_x$; therefore, one can also rise the question of differentiability of $\theta(x, t)$ with respect to time.

Let us consider smoothness of the temporal evolution of Eq. (1). Nonsmoothness is associated with the highest-order derivatives with respect to x and noise in $q(x)$ and the impact of the advection is of interest—since for $u = 0$ only time-independent patterns are stable. Meanwhile, the nonlinear term makes a trivial influence on the dynamics of system (1) by preventing an infinite growth of excited patterns. Hence, addressing the issue of the smoothness of temporal evolution of $\theta(x, t)$, we can omit the nonlinear term and consider linear equation

$$\dot{\theta} = (-u\theta - \theta_{xxx} - q(x)\theta_x)_x. \quad (4)$$

One can consider an eigen-mode of the latter equation $\theta = \Theta(x) e^{\lambda t}$. Similarly to the classical Anderson localization, in our case any eigen-mode $\Theta(x)$ is exponentially localized in space [10] (see Fig. 2 for illustration as well). For the eigen-mode, Eq. (4) reads

$$\lambda\Theta = -u\Theta_x - \Theta_{xxx} - (q(x)\Theta_x)_x.$$

Multiplying the latter equation by $\Theta^*(x)$ and integrating over x , performing similar manipulations for its complex-conjugate and employing partial integration, one can obtain

$$\operatorname{Re}(\lambda) \|\Theta\|^2 = -\|\Theta_{xx}\|^2 + \|q(x)\Theta_x\|^2, \quad (5)$$

$$\operatorname{Im}(\lambda) \|\Theta\|^2 = -2u \|\operatorname{Re}(\Theta) \operatorname{Im}(\Theta)\|, \quad (6)$$

where $\|\dots\| \equiv \int_{-\infty}^{+\infty} \dots dx$. One can rewrite equation (5) as

$$\operatorname{Re}(\lambda) \|\Theta\|^2 = -\|\Theta_{xx}\|^2 + q_0 \|\Theta_x\|^2 - \sigma \|W(x)(|\Theta_x|^2)_x\|, \quad (7)$$

where $W(x) = \int^x \xi(x_1) dx_1$ is a Wiener process, which is a finite random number for finite x . If $\Theta_x(x)$ is differentiable, i.e., $\Theta_{xx}(x)$ is finite, then $(|\Theta_x|^2)_x$ is finite and thus all terms in the r.h.s. of (7) are finite; therefore, $\operatorname{Re}(\lambda)$ is finite. Simultaneously, according to (6), $\operatorname{Im}(\lambda)$ should be finite. If we now admit $\Theta_{xx}(x)$ to tend to infinity, then $\|\Theta_{xx}\|^2$ diverges as the square of Θ_{xx} , while $\|W(x)(|\Theta_x|^2)_x\|$ diverges linearly in Θ_{xx} , which—due to positivity of $\|\Theta_{xx}\|^2$ and $\|\Theta\|^2$ —means that $\operatorname{Re}(\lambda) \rightarrow -\infty$. Thus, the eigen-modes with diverging $\Theta_{xx}(x)$ decay infinitely fast in time. To conclude, the eigen-modes either evolve with finite values of λ or, with diverging $\Theta_{xx}(x)$, decay infinitely fast and do not contribute the system dynamics at finite time scales. As any initial state can be decomposed into eigen-modes, the temporal evolution of the system must be infinitely smooth after a vanishingly short transient period.

This property of smoothness of the dependence on one coordinate (time for (4)) in spite of the disorder and nonsmoothness in the dependence on the other coordinate (spatial coordinate x for (4)) is not pertaining uniquely to the system we consider. One can recall a “mirror” situation for the dynamics of an ensemble of oscillators with identical or slightly non-identical parameters, subject to identical common noise $\xi(t)$. For such ensembles in [21, 22], the notion of a snapshot attractor—the ensemble state at certain instant of time—has been introduced. In spite of random non-smooth dynamics of oscillators in time, the snapshot attractors, which represent a kind of a spatial pattern, turn out to be smooth and regular (can be fractal, but still regular with a fine structure) [21, 22, 23, 24]. Here, the situation is similar to the case of Eq. (1) up to the interchange of the space and time coordinates.

2.2. Bifurcation scenarios

In numerical simulations we observed only two bifurcation scenarios of advective suppression of localized convective patterns. Scenario I is trivial; the stable patterns remains time-independent for all values of u , the pattern amplitude monotonously decreases with increasing u and at certain value u_{cr} the stable convective patterns disappears via a pitchfork bifurcation (Fig. 3a). The bifurcation is a pitchfork one due to the symmetry $\theta \leftrightarrow -\theta$.

Let us now consider a complex scenario II for a sample realization of $q(x)$ shown in Fig. 5a and periodic lateral boundary conditions. In Figs. 3b–d, the temperature altitude $[\theta]$ of the stable convective patterns is plotted vs advection strength u and the stability properties of these patterns and the trivial state are presented. In Fig. 3b, one can see that the time-independent solution, which exists at $u = 0$, becomes unstable for advection u strong enough. Meanwhile, some stable oscillatory regime emerges in the system. There is a hysteresis of the transition between these two regimes. With further increase of the advection strength u the oscillation amplitude decreases, until the oscillatory regime disappears via a Hopf bifurcation at u_{cr} ; u_{cr} is the critical strength of advection required for suppression of the localized convective pattern.

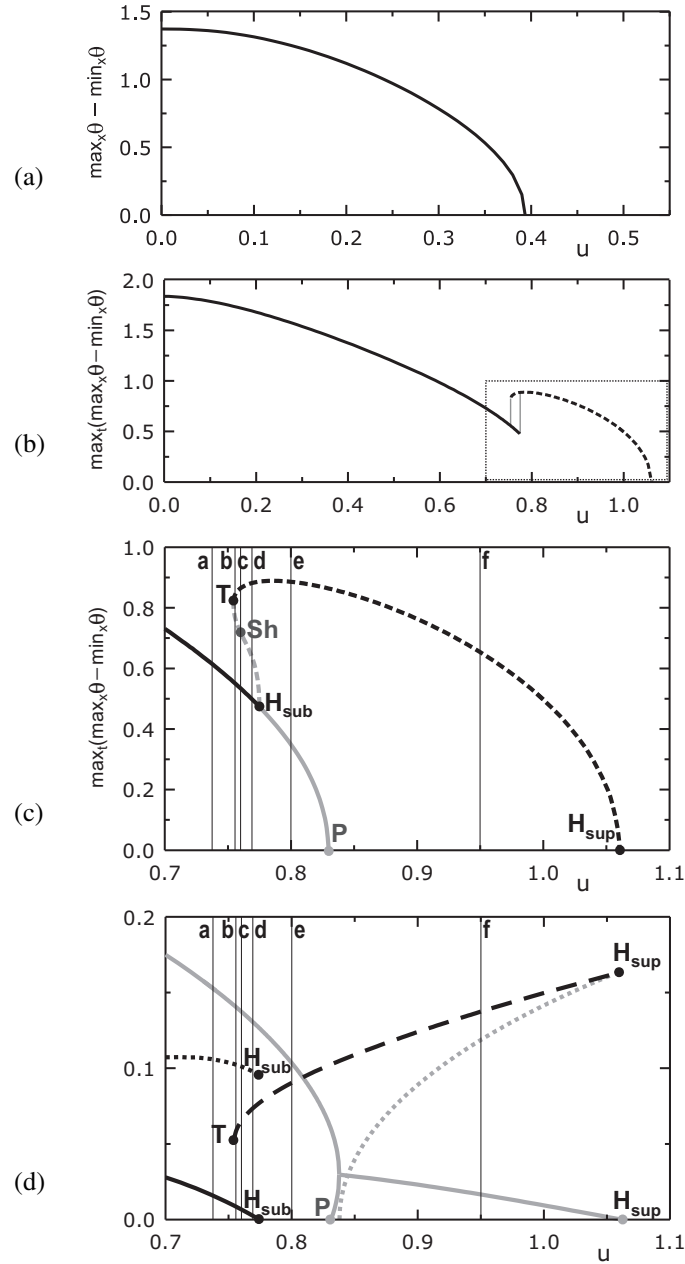


Figure 3: **Scenario I:** (a) The altitude of the temperature field of a localized pattern for a sample realization of noise is plotted vs advection strength u . The pattern is time-independent for all u . **Scenario II:** (b) The altitude of the temperature field $[\theta]$ of the time-independent stable pattern (solid line) and the maximal value of $[\theta]$ for the stable oscillatory regime (dashed line) are plotted vs advection strength u for a sample realization of $q(x)$ presented in Fig. 5a. (c) Zoom-in of the region marked in plot (b), gray lines show unstable regimes. (d) Black lines: the exponential decay rate (solid line) and the frequency (dotted line) of perturbations of the time-independent pattern and the frequency of the stable oscillatory flow (dashed line), gray lines: the exponential growth rate (solid) and the frequency (dotted) of perturbations of the trivial state. For the values of u marked by vertical lines with letters in plots (c,d), projections of the phase portraits are shown in Fig. 4 under the corresponding letters.

For a comprehensive understanding of this bifurcation scenario, we provide a zoom-in of the amplitude diagram of the observed regimes in Fig. 3c and the linear stability analysis of the observed regimes in Fig. 3d. Close to point **P** the exponential growth rate of the linear perturbations of the trivial state is small and turns complex (gray curves in Fig. 3d). Hence, the system is close to a co-dimension 2 bifurcation where two real eigenvalues of the linear stability

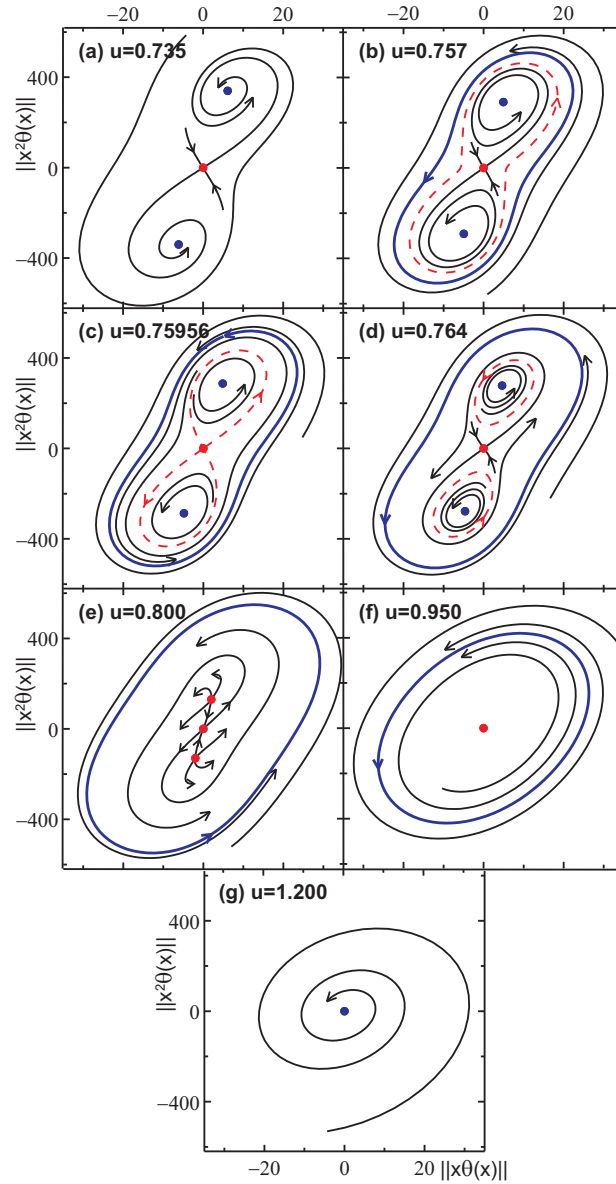


Figure 4: Cascade of the projections of the phase trajectories of system (1) onto the plane $(\|x\theta\|, \|x^2\theta\|)$ for $q(x)$ plotted in Fig. 5a and specified values of advective through-flow u .

problem turn to zero, but this bifurcation differs from a Bogdanov–Takens one [25] due to the sign inversion symmetry ($\theta \rightarrow -\theta$) of our system. Such a situation (being close to a Bogdanov–Takens bifurcation modified by the sign inversion symmetry) is widespread in fluid dynamics; *e.g.*, Knobloch and Proctor have encountered it for the problem of convection in the presence of an imposed vertical magnetic field [26]. On some stages of the bifurcation scenario the principal manifold of the system is two-dimensional (cf [26]) and, therefore, the minimal dimension required for the presentation of the system dynamics is 2. We project the system trajectories onto the plane $(\|x\theta\|, \|x^2\theta\|)$ for presentation in Fig. 4 (here $\|\dots\| \equiv \int_{-L_{\text{layer}}/2}^{L_{\text{layer}}/2} \dots dx$ stands for the integration over the calculation domain of length L_{layer}); linear in θ quantifiers $\|x\theta\|$ and $\|x^2\theta\|$ are the simplest independent integral quantifiers of pattern $\theta(x)$.

In the absence of advection, only time-independent convective patterns can arise. For small u , this holds true by continuity (Fig. 4a). As advection becomes stronger, a pair of finite-amplitude time-periodic regimes (Fig. 4b)

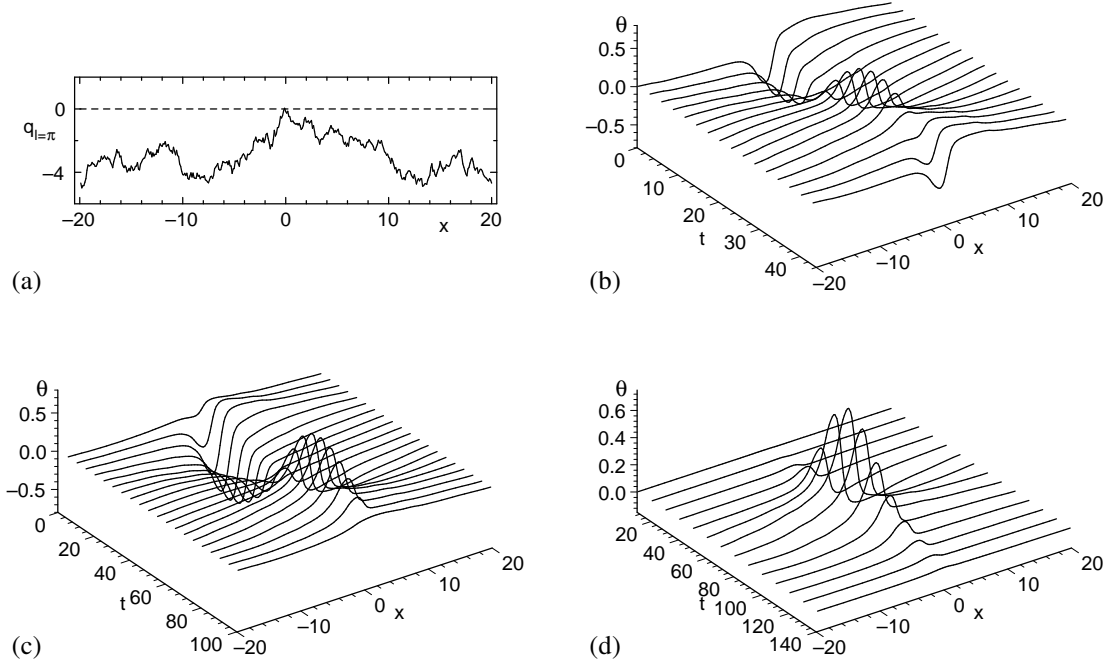


Figure 5: Dynamics of field $\theta(x, t)$ is presented for the sample realization of $q(x)$ plotted in (a). (b): the stable time-periodic pattern at $u = 0.95$, (c,d): the stable time-periodic pattern and the homoclinic pattern at $u_{Sh} \approx 0.75956$, respectively.

appears at $u = u_T \approx 0.754$ via a tangential bifurcation (point **T** in Figs. 3c,d); the more intense periodic pattern is locally stable (Fig. 4b, solid loop: stable limit cycle, dashed curve: saddle cycle). At $u_{Sh} \approx 0.75956$ (**Sh** in Fig. 3c), the unstable manifold of the trivial state intersects the stable one, and two homoclinic loops form (see Fig. 4c, in Fig. 5d the temporal evolution of the homoclinic solution is presented); the union of these loops is the former unstable cycle. In Fig. 4c, simultaneously with these repelling loops, the locally stable periodic (Fig. 5c) and time-independent patterns can be seen; the homoclinic loops belong to the boundary between the attraction basins of these stable regimes. For stronger advection, $u_{Sh} < u < u_{H_{sub}}$, the homoclinic loops turn into a pair of unstable cycles (Fig. 4d). This bifurcation of homoclinic trajectories somewhat differs from a general bifurcation described by the Shil'nikov's theorem [27, 25] due to the symmetry $\theta \rightarrow -\theta$; here the cycles exist on both sides of the bifurcation point, while for the Shil'nikov's case the cycle exists only on one side. Further, the unstable cycles shrink as u increases and collapse onto the time-independent solutions making them unstable via a subcritical Hopf bifurcations at $u_{H_{sub}} \approx 0.775$ (**H_{sub}** in Figs. 3c,d). For $u_{H_{sub}} < u < u_{H_{sup}}$, the only stable regime is the time-periodic pattern (Figs. 4e,f, 5b). Within this range of u , at $u_P \approx 0.832$, the unstable time-independent patterns disappear via a pitchfork bifurcation near the trivial state (**P** in Figs. 3c,d), turning it from a saddle into an unstable focus (Fig. 4f). For $u > u_P$, increase of u leads to the shrinking of the limit cycle till the time-periodic pattern diminishes to zero at $u_{H_{sup}} \approx 1.062$ and disappears via a supercritical Hopf bifurcation (**H_{sup}** in Figs. 3c,d). For $u > u_{H_{sup}}$, all convective currents decay (Fig. 4g). Noticeably, the vicinity of trivial state belongs to the attraction basin of the time-independent patterns for $u < u_{Sh}$ and to the one of the time-periodic pattern for $u_{Sh} < u < u_{H_{sup}}$, which determines whether small initial perturbations of the no-flow state evolve to the former regime or to the latter.

The difference in the scenarios of advective suppression for two groups of localized patterns rises the natural question whether these patterns can be distinguished at $u = 0$ and what (if any) can be an appropriate discrimination characteristic. In Fig. 6, integral characteristics of localized patterns observed in numerical simulations are plotted for $q_0 = -3$. In Fig. 6a, one can see, that for $u = 0$ the flow intensity $\|\theta_x^2\| \propto [\theta]^2$ and the proportionality coefficient, as well as the dispersion around the trend $\|\theta_x^2\| = k[\theta]^2$, are similar for both the patterns disappearing via a pitchfork bifurcation (scenario I) and a Hopf one (scenario II), meaning the patterns of these two types can be hardly distinguished by their simplest shape properties. In Figs. 6b and c, one can see that critical values u_{cr} for a given value of $[\theta]$ or $\|\theta_x^2\|$ are

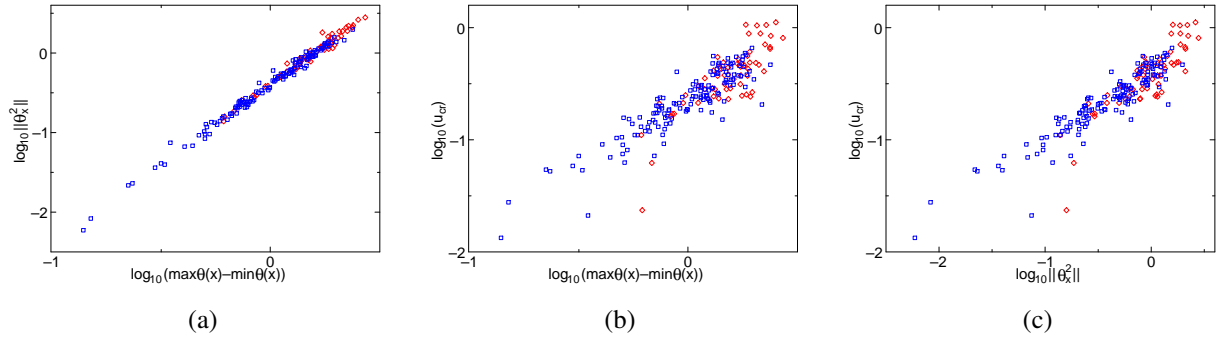


Figure 6: Integral characteristics of localized patterns at $q_0 = -3$, $u = 0$. (a): flow intensity $\|\theta_x^2\|$ vs temperature altitude $[\theta]$; (b) and (c): critical advection strength u_{cr} vs $[\theta]$ and $\|\theta_x^2\|$, respectively. Blue squares: the convective pattern disappears via a pitchfork bifurcation, red diamonds: via a Hopf bifurcation.

strongly dispersed—almost by an order of magnitude. Thus, the primary quantifiers of the pattern intensity are very far from being sufficient for prediction of the advection strength required for the pattern suppression. The only reliable conclusion which can be drawn from the numerical results plotted in Fig. 6 is that intense patterns more frequently disappear via a Hopf bifurcation, while for the low-intensity patterns a pitchfork bifurcation is more typical. However, this qualitative discrepancy is quite weak; the majorities of both scenarios are observed in the range of intensities where they coexist. To conclude, the correlation between scenarios of advective suppression and integral quantifiers of the convective pattern intensity turns out to be not playing a decisive role.

3. Two-mode model reduction

For better understanding of these scenarios and interrelations between them, let us analyse the model reduction admitting comprehensive consideration.

3.1. Derivation of model reduction equations

Let us consider a localized pattern in system (1). This localized pattern onsets where the ground state of the system is unstable. Mathematically it means that the linearized equation (4) possesses a spatially localized instability mode. The localized solutions are of interest when they are sparse in space, which is the case of non-small negative q_0 (see Fig. 2 and [10]); therefore, one can rarely observe more than one instability mode at certain excitation centre. Thus, we rewrite Eq. (1) as

$$\dot{\theta} = -u\theta_x + \hat{L}\theta + ((\theta_x)^3)_x, \quad (8)$$

where

$$\hat{L}f \equiv -f_{xxxx} - (q(x)f_x)_x, \quad (9)$$

and assume only one instability mode at $u = 0$;

$$\hat{L}\theta_\lambda(x) = \lambda\theta_\lambda(x) \quad (10)$$

with $\lambda > 0$. In Sec. 2.1, we demonstrated that the exponential growth rate λ is real-valued at $u = 0$ (in Eq. (6), $\text{Im}(\lambda) \propto u$).

The nonlinear term in Eq. (8) prevents the instability mode from infinite growth, resulting in saturation, while advection u affects the shape of the pattern. Specifically, the u -term makes contribution $-u\theta_x$ into the time-derivative $\dot{\theta}$. Hence, for non-large u and λ , the shape of the temperature field is contributed by the principal part $\propto \theta_\lambda(x)$ and perturbed by θ_x ; a sound approximation for the temperature field becomes

$$\theta(x, t) \approx a(t)\theta_\lambda(x) + b(t)\theta'_\lambda(x), \quad (11)$$

(henceforth, the prime stands for the x -derivative). Eq. (8) with temperature field (11) can be projected onto $\theta_\lambda(x)$ and $\theta'_\lambda(x)$ with a standard definition of the inner product; one finds

$$a \|\theta_\lambda^2\| = ub \|\theta'_\lambda\|^2 + \lambda a \|\theta_\lambda^2\| - a^3 \|\theta'_\lambda\|^4 - 3ab^2 \|\theta'_\lambda\|^2 \|\theta'_\lambda\|^2 - b^3 \|\theta'_\lambda\|^3, \quad (12)$$

$$b \|\theta'_\lambda\|^2 = -ua \|\theta'_\lambda\|^2 + b \|\theta'_\lambda \hat{L}\theta'_\lambda\| - 3a^2b \|\theta'_\lambda\|^2 \|\theta'_\lambda\|^2 - 3ab^2 \|\theta'_\lambda\|^3 - b^3 \|\theta'_\lambda\|^4. \quad (13)$$

Here partial integration has been employed to evaluate the following integrals:

$$\begin{aligned} \|\theta_\lambda \theta'_\lambda\| &= \|(\theta_\lambda^2/2)'\| = (\theta_\lambda^2/2)|_{-\infty}^{+\infty} = 0, \\ \|\theta_\lambda \theta'_\lambda\| &= -\|\theta'_\lambda\|^2, \\ \|\theta_\lambda \hat{L}\theta'_\lambda\| &= \|(\hat{L}\theta_\lambda) \theta'_\lambda\| = \lambda \|\theta_\lambda \theta'_\lambda\| = 0, \\ \|\theta_\lambda ((\theta')^3)'\| &= -\|\theta'_\lambda (\theta')^3\| = -a^3 \|\theta'_\lambda\|^4 - 3a^2b \|\theta'_\lambda\|^3 \|\theta'_\lambda\| - 3ab^2 \|\theta'_\lambda\|^2 \|\theta'_\lambda\|^2 - b^3 \|\theta'_\lambda\|^3, \\ \|\theta'_\lambda ((\theta')^3)'\| &= -\|\theta'_\lambda (\theta')^3\| = -a^3 \|\theta'_\lambda\|^3 \|\theta'_\lambda\| - 3a^2b \|\theta'_\lambda\|^2 \|\theta'_\lambda\|^2 - 3ab^2 \|\theta'_\lambda\|^3 - b^3 \|\theta'_\lambda\|^4, \end{aligned}$$

where $\|(\theta'_\lambda)^3 \theta'_\lambda\| = \|((\theta'_\lambda)^4/4)'\| = (\theta'_\lambda^4/4)|_{-\infty}^{+\infty} = 0$.

Let us notice that the integral $\|\theta'_\lambda (\theta')^3\|$ turns to zero for both even and odd functions $\theta_\lambda(x)$, meaning that this integral represents a symmetry defect of the mode, while all the other coefficients of nonlinear terms have non-negative integrands. Hence, one can typically expect integral $\|\theta'_\lambda (\theta')^3\|$ to be small compared to other integrals. Indeed, specifically for the noise realization presented in Fig. 2 for $q_0 = -2.5$, the numerical calculation of integrals yields $\|(\theta'_\lambda)^4\| \approx 0.0682$, $\|(\theta'_\lambda)^2 (\theta'_\lambda)^2\| \approx 0.0561$, $\|\theta'_\lambda (\theta')^3\| \approx -0.0059$, $\|(\theta'_\lambda)^4\| \approx 0.1198$; the absolute value of the integral under discussion is by one order of magnitude smaller than the other integrals. For the further analysis we will set this integral to zero for simplicity without loss of generality.

In terms of

$$\tau = \lambda t, \quad A = a \sqrt{\frac{\|(\theta'_\lambda)^4\|}{\lambda \|\theta_\lambda^2\|}}, \quad B = b \sqrt{\frac{\|(\theta'_\lambda)^4\|}{\lambda \|\theta'_\lambda\|^2}}, \quad U = \frac{u}{\lambda} \sqrt{\frac{\|(\theta'_\lambda)^2\|}{\|\theta_\lambda^2\|}}$$

Eqs. (12)–(13) read

$$\dot{A} = A + UB - A^3 - 3AB^2 \frac{\|(\theta'_\lambda)^2 (\theta'_\lambda)^2\| \|\theta'_\lambda\|^2}{\|(\theta'_\lambda)^4\| \|\theta_\lambda^2\|}, \quad (14)$$

$$\dot{B} = -UA + \frac{\|\theta'_\lambda \hat{L}\theta'_\lambda\|}{\lambda \|\theta'_\lambda\|^2} B - 3A^2 B \frac{\|(\theta'_\lambda)^2 (\theta'_\lambda)^2\| \|\theta'_\lambda\|^2}{\|(\theta'_\lambda)^4\| \|\theta'_\lambda\|^2} - B^3 \frac{\|(\theta'_\lambda)^4\|}{\|(\theta'_\lambda)^4\|}. \quad (15)$$

For large negative q_0 , when the pattern excitation centres are rare, the probability of heaving the growth rate λ rapidly decreases with the increase of λ ; small values of λ are abundant, while large values of λ are nearly improbable. Simultaneously, other modes are rapidly decaying and a large decay rate ($-\|\theta'_\lambda \hat{L}\theta'_\lambda\|/\|(\theta'_\lambda)^2\|$) of B should be typical. Hence, the coefficient

$$K \equiv \frac{-\|\theta'_\lambda \hat{L}\theta'_\lambda\|}{\lambda \|\theta'_\lambda\|^2}$$

is typically large. Specifically for the noise realization presented in Fig. 2 for $q_0 = -2.5$, numerical calculations yield $\|\theta'_\lambda \hat{L}\theta'_\lambda\|/\|(\theta'_\lambda)^2\| \approx -13.95$, which is large negative, and $\lambda \approx 0.2407$, which is small positive, as expected.

The nonlinear terms in Eqs. (14)–(15) are purely dissipative. While for the excited mode A the nonlinearity deters the growth, the eigen dynamics of perturbation B is a rapid decay (K is large), which is only facilitated by nonlinear terms. The mode B experiencing a strong dumping is pushed from the zero-state merely by the advection term UA . Hence, B should be small compared to A and one can neglect all the nonlinear terms except for the leading one A^3 .

Finally, the model reduction equations relevant for typical localized patterns can be written-down as

$$\dot{A} = A + UB - A^3, \quad (16)$$

$$\dot{B} = -UA - KB. \quad (17)$$

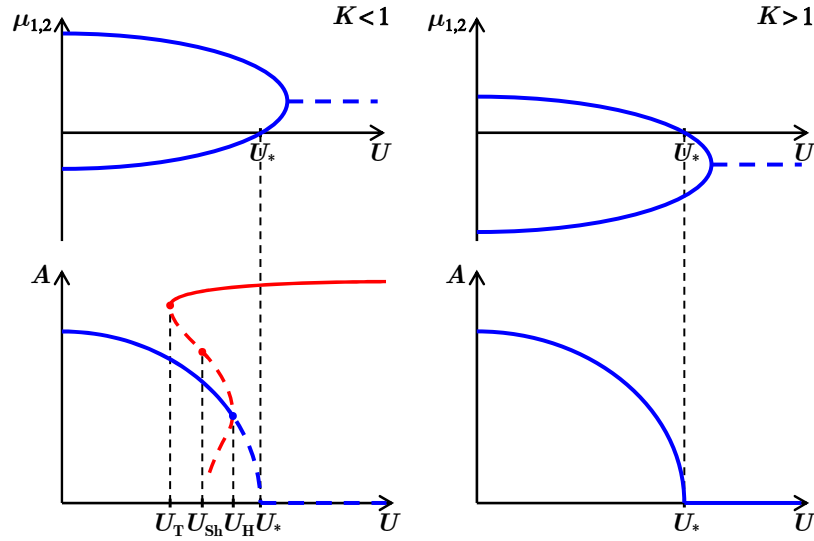


Figure 7: The dependence of the stability properties of the trivial state of the dynamic system (16)–(17) on U is plotted in the upper graphs for $K < 1$ and $K > 1$. The corresponding finite-amplitude regimes of the system dynamics are presented in the lower graphs. The system dynamics for $K < 1$ is shown in further detail in Fig. 8.

3.2. Dynamics of reduced model (16)–(17)

System (16)–(17) admits two time-independent solutions: the trivial ground state $A = B = 0$ and a nontrivial state

$$A_0 = \pm \sqrt{1 - \frac{U^2}{K}}, \quad B_0 = -\frac{U}{K} A_0. \quad (18)$$

The nontrivial state apparently exists for

$$U < U_* = \sqrt{K}$$

and disappears via a subcritical pitchfork bifurcation at U_* .

The stability analysis for the trivial state can be performed analytically and yields the exponential growth rates of linear perturbations

$$\mu_{1,2} = \frac{1-K}{2} \pm \sqrt{\frac{(1+K)^2}{4} - U^2}. \quad (19)$$

Exponents $\mu_{1,2}$ are real for

$$U < U_{k-f} = \frac{1+K}{2}$$

and one of them changes its sign at $U_* = \sqrt{K}$ (Fig. 7). For $U > U_{k-f}$, the exponents form a complex conjugate pair with real part $\text{Re}(\mu_{1,2}) = (1-K)/2$, which is positive for $K < 1$ and negative for $K > 1$.

Comprehensive bifurcational analysis can be performed for the dynamic system (16)–(17). It reveals the possibility of only two scenarios depending on K :

(I) For $K > 1$ (Fig. 7), the time-independent patterns are the only stable states; the nontrivial solutions disappear via a pitchfork bifurcation at $U = U_*$.

(II) For $K < 1$, the sequence of bifurcations is more complex but still universal (see Fig. 8).

For the Hopf bifurcation the threshold can be calculated analytically:

$$U_H = \sqrt{K(K+2)/3}.$$

One can see, that the picture of bifurcational scenarios of the reduced model resembles that of the original model. The only qualitative difference is the lack of a slow decline of the real part of the exponential growth rate of the linear

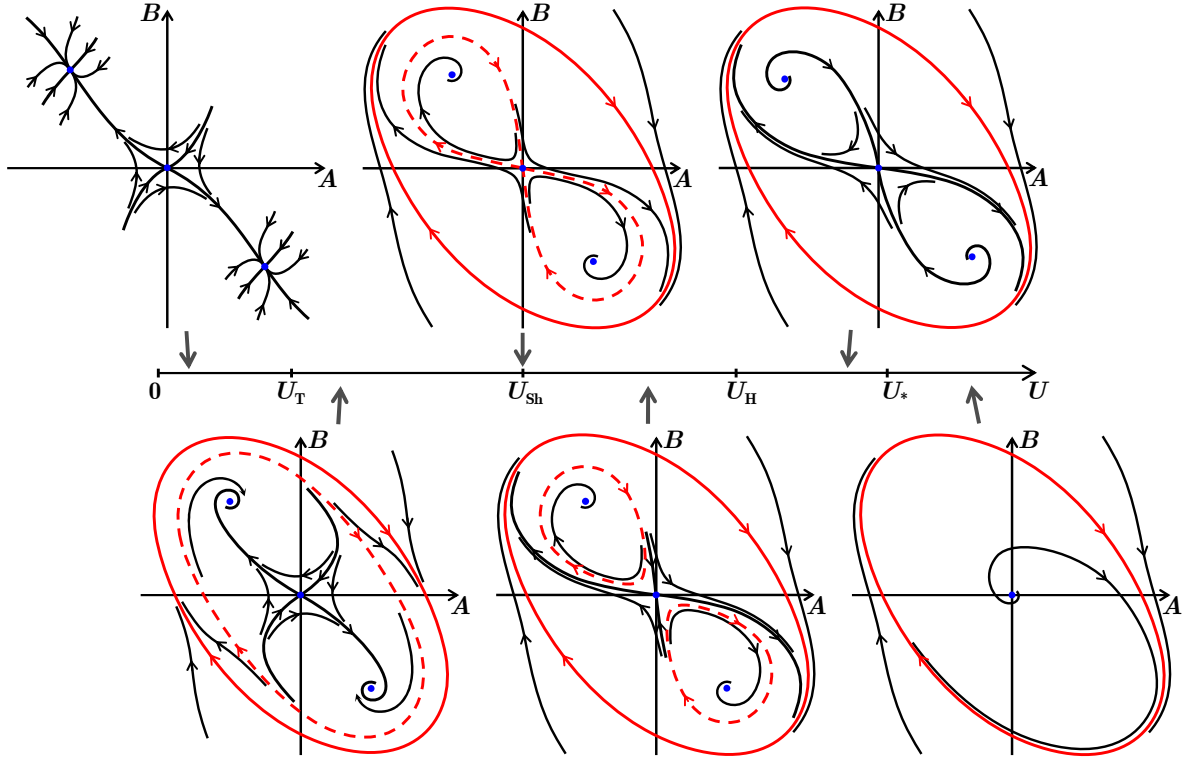


Figure 8: The bifurcational scenario of the dynamic system (16)–(17) is presented for $K < 1$. Next to $U = 0$, there are three fixed points in the phase space; two nontrivial ones are attracting. At U_T the pair of stable and unstable cycles arises around these fixed points (the red solid and dashed closed curves, respectively) via a tangential bifurcation. As U increases, the outer stable cycle slightly grows, while the inner unstable one shrinks, until it turns into two homoclinic loops at U_{Sh} and further splits into two separate unstable cycles for $U > U_{Sh}$. At U_H the unstable cycles disappear via a subcritical Hopf bifurcation and make the time-independent nontrivial states unstable. Further, the unstable nontrivial time-independent states disappear via a pitchfork bifurcation at U_* , although this does not influence the observable stable regimes of the system. Further increase of U does not lead to any qualitative changes in the system dynamics.

perturbations, which can be seen in Fig. 3d with a gray line crossing the abscissa at \mathbf{H}_{sup} . This decline leads to the decay of the oscillatory regime for increasing u ; in the reduced model, this decay turns out to be not represented, and oscillatory regime in scenario II persists for large U . Otherwise, the scenario II in the reduced model resembles all fine features of the scenario II in the original system. Thus, the model reduction firstly validates the completeness of the reported picture of scenarios in the original system and secondly sheds light onto the nature of the bifurcational scenarios in the original model. The underlying difference between two scenarios turns out to be quite simple; the pair of perturbation modes of the trivial state becomes coupled by advection u and converges as u increases (see the upper graphs in Fig. 7). When the sum of the real parts of the exponential growth rates of modes is negative ($1 - K < 0$), the convergence leads to a plain decay of both modes. When the sum is positive ($1 - K > 0$), a reacher sequence of bifurcations must occur near U_* .

4. Conclusion

We have considered the effect of an imposed advection on the localized patterns excited in the modified Kuramoto–Sivashinsky equation (with symmetry $\theta \leftrightarrow -\theta$) under frozen parametric disorder. Firstly, we have revealed that the system evolution is infinitely smooth in time even though the frozen parametric noise is δ -correlated in space. Secondly, while all the stable regimes in the advection-free system are time-independent, stable oscillatory regimes may appear in the presence of advection. Thirdly, two scenarios of advective suppression (“washing-out” from the excitation centres) of localized patterns have been found with numerical simulation. In scenario I, the stable patterns remain time-independent for all u and disappear via a pitchfork bifurcation. In scenario II, a strong advection results

in appearance of a stable oscillatory regime, which arises via a tangential bifurcation of cycles. In certain range of advection strength u , one observes hysteresis between stable oscillatory and time-independent regimes. For a stronger advection the time-independent regimes become unstable via a subcritical Hopf bifurcation and the oscillatory regime becomes the only attractor in the system. With the further increase of the advection strength, the oscillating regime gradually decays until it disappears via a Hopf bifurcation. Fourthly, we have derived a two-mode reduced model and performed its comprehensive bifurcational analysis, which has yielded that only two reported bifurcation scenarios are possible in the system and revealed the underlying difference between them. With this analysis one can see, that in spite of a seeming complexity of the second scenario, a pair of these scenarios is the simplest possible picture for the effect of the advection, which couples two originally-monotonous modes of perturbations of the trivial state, on the dynamics of a system of the given kind.

Acknowledgements

The author is thankful to A.V. Pimenova for useful comments and discussions. The work has been supported by the Russian Science Foundation (Grant No. 14-21-00090).

References

- [1] Anderson PW. Absence of Diffusion in Certain Random Lattices. *Phys Rev* 1958;109:1492–505.
- [2] Abrahams E, Anderson PW, Licciardello DC, Ramakrishnan TV. Scaling Theory of Localization: Absence of Quantum Diffusion in Two Dimensions. *Phys Rev Lett* 1979;42:673–6.
- [3] John S. Strong localization of photons in certain disordered dielectric superlattices. *Phys Rev Lett* 1987;58:2486–9.
- [4] Schwartz T, Bartal G, Fishman S, Segev M. Transport and Anderson localization in disordered two-dimensional photonic lattices. *Nature* 2007;446:52–55.
- [5] Klyatskin VI. *Dynamics of Stochastic Systems*. Amsterdam: Elsevier; 2005.
- [6] Maynard JD. Colloquium: Acoustical analogs of condensed-matter problems. *Rev Mod Phys* 2001;73:401–17.
- [7] Fröhlich J, Spencer T. A rigorous approach to Anderson localization. *Phys Rep* 1984;103:9–25.
- [8] Lifshitz IM, Gredeskul SA, Pastur LA. *Introduction to the Theory of Disordered Systems*. New York: Wiley; 1988.
- [9] Gredeskul SA, Kivshar YS. Propagation and scattering of nonlinear waves in disordered systems. *Phys Rep* 1992;216:1–61.
- [10] Goldobin DS, Shklyaeva EV. Localization and advective spreading of convective currents under parametric disorder. *J Stat Mech* 2013;09:P09027.
- [11] Goldobin DS, Shklyaeva EV. Diffusion of a passive scalar by convective flows under parametric disorder. *J Stat Mech* 2009;01:P01024.
- [12] Goldobin DS. Advective enhancement of eddy diffusivity under parametric disorder. *Phys Scr* 2010;T142:014050.
- [13] Hammele M, Schuler S, Zimmermann W. Effects of parametric disorder on a stationary bifurcation. *Phys D* 2006;218:139–57.
- [14] Limi M, Kofane T. Parametric disorder effects on a subcritical stationary bifurcation. *Int J Nonlinear Mech* 2016;82:75–82.
- [15] Goldobin DS, Shklyaeva EV. Large-Scale Thermal Convection in a Horizontal Porous Layer. *Phys Rev E* 2008;78:027301.
- [16] Knobloch E. Pattern selection in long-wavelength convection. *Phys D* 1990;41:450–79.
- [17] Shtilman L, Sivashinsky G. Hexagonal structure of large-scale Marangoni convection. *Phys D* 1990;52:477–88.
- [18] Hoyle RB. Zigzag and Eckhaus instabilities in a quintic-order nonvariational Ginzburg-Landau equation. *Phys Rev E* 1998;58:7315–8.
- [19] Schöpf W, Zimmermann W. Multicritical behaviour in binary fluid convection. *Europhys Lett* 1989;8:41–6.
- [20] Schöpf W, Zimmermann W. Convection in binary fluids: amplitude equations, codimension-2 bifurcation, and thermal fluctuations. *Phys Rev E* 1993;47:1739–64.
- [21] Yu L, Ott E, Chen Q. Transition to Chaos for Random Dynamical Systems. *Phys Rev Lett* 1990;65:2935–8.
- [22] Yu L, Ott E, Chen Q. Fractal distribution of floaters on a fluid surface and the transition to chaos for random maps. *Phys D* 1991;53:102–24.
- [23] Goldobin DS, Pikovsky A. Synchronization and desynchronization of self-sustained oscillators by common noise. *Phys Rev E* 2005;71:045201.
- [24] Goldobin DS. Coherence versus reliability of stochastic oscillators with delayed feedback. *Phys Rev E* 2008;78:060104.
- [25] Kuznetsov YA. *Elements of Applied Bifurcation Theory*. New York: Springer; 2004.
- [26] Knobloch E, Proctor M. Nonlinear periodic convection in double-diffusive systems. *J Fluid Mech* 1981;108:291–316.
- [27] Shil'nikov LP. On the generation of a periodic motion from a trajectory which leaves and re-enters a saddle-saddle state of equilibrium. *Soviet Math Dokl* 1966;7:1155–8.